

Synthesis of Anisotropic Mesostructured Gold Electrodeposits

M. Saitou

Department of Mechanical Systems Engineering, University of the Ryukyus, 1 Senbaru Nishihara-cho Okinawa, 903-0213, Japan

E-mail: saitou@tec.u-ryukyu.ac.jp

Received: 5 May 2016 / Accepted: 8 May 2016 / Published: 7 July 2016

Anisotropic mesostructured gold electrodeposits were synthesized on an indium tin oxide (ITO) glass from a solution of sodium disulfiteaurate (I) by a rectangular pulse current technique. Characterization of the gold electrodeposit was performed using a scanning electron microscope (SEM), X-ray diffraction (XRD), and energy dispersive X-ray spectrometry (EDX). Two shapes of the gold electrodeposits, which change with the solution temperature and the amplitude of the rectangular pulse current, are obtained; one is a star-like concave polygon with a lot of horn and the other is a truncated pyramid-like configuration. A gold thin film comprising of the star-like gold electrodeposit includes a large number of mesostructured pores. The pyramid-like electrodeposit has four triangular (111) planes. The gold electrodeposits are shown to be purely made of gold by the EDX measurement. The XRD measurement reveals a texture change in the gold thin film from the (111) plane to the (110) one with the growth time, whereas the surface morphology obeys the surface energy minimum.

Keywords: star-like gold electrodeposit, pyramid-like gold electrodeposit, texture coefficient, sodium disulfiteaurate (I), surface energy minimum

1. INTRODUCTION

Anisotropic mesostructured gold materials [1] that exhibit extraordinary properties in catalysis, optics, and surface plasmon have been fascinated in a field of science and technology. The attractive property originates in the complicated configuration of the mesostructured gold materials. As reproducible synthesis methods for the gold material are required to investigate the extraordinary property, many kinds of the synthesis methods [2-6] have already been proposed.

One of the useful methods is an electrodeposition technique [7] that has a wide variety of choice in electrolyte, deposition process, and additives. Many efforts have primarily been made to

generate a gold thin film with a morphological smooth surface [8-9]. Unfortunately, there are only very few studies that focused on the anisotropic mesostructured gold electrodeposit insofar as we know.

Gold materials ranging in size from nanometer to micron meter, i.e., the mesostructured gold materials have a configuration bounded by crystallographic planes [5, 10]. The plane that emerges in a growth process lowers the total surface free energy when the surface energy minimum dominates the grown condition in the synthesis of the gold material [11-12]. In face centered cubic (FCC) metals, the (111) plane is well known to have the minimum surface energy. However, the formation process of the mesostructured gold materials is so complicated that only the (111) plane is not always observed as the surface configuration [1, 4]. In addition, in electrodeposition, the exchange current density [13, 14] that indicates a rate of the electron transfer reaction between a gold ion in a solution and an electrode surface should be considered because the rate is dependent on the crystallographic plane of electrodeposits. For example, the (110) plane in gold [13] has the maximum exchange current density, which means that the (110) plane makes it possible to have the highest growth rate. Hence, the surface configuration of the mesostructured gold electrodeposit may be understood from the viewpoints of the surface energy and the exchange current density.

In order to synthesize the mesostructured gold electrodeposit with high purity [7, 15], it is very important to choose the type of a gold electrodepositing solution. If the solution has the current efficiency that is almost 100%, impurities such as hydrogen and sulfur cannot be incorporated into the gold electrodeposit. In addition, a pulse current technique in gold electrodeposition has an advantage in reducing impurities in the gold electrodeposit [16]. In this study, a sodium disulfitoaurate (I) solution that has about 100% current efficiency and a rectangular pulse current technique were chosen.

In the present study, we demonstrate the synthesis and development of the anisotropic mesostructured gold electrodeposit characterized by SEM, EDX, and XRD.

2. EXPERIMENTAL SET UP

The experiment was performed as follows; An ITO glass (sheet resistance 6Ω) $10 \times 10 \text{ mm}^2$ and carbon plate of $35 \times 40 \text{ mm}^2$ were prepared for a cathode and anode electrode. The area of the carbon plate is 14 times larger than that of the ITO glass. Hence, the impedance of the electric double layer formed between the carbon plate and a gold electrodeposition solution can be ignored. An electrochemical cell including a 0.3 mol/L solution of sodium disulfitoaurate (I) ($\text{AuNa}_3\text{O}_3\text{S}_2$) was held at a temperature of 303 K or 323 K.

The rectangular pulse voltage at a frequency of 50 kHz was supplied with a function generator. To measure a rectangular pulse current passing through the electrochemical cell with a digital oscilloscope, a metal film resistor (KOA Corporation) of 51Ω was connected in series with the electrochemical cell. The amplitudes of the rectangular pulse current were 4.7, 7.7, and 14.4 mA/cm^2 . Figure 1 shows a typical rectangular pulse current having a frequency of 50 kHz and an amplitude of 14.4 mA/cm^2 . The current on-time was chosen to be equal to the current off-time.

After electrodeposition, the gold electrodeposit on the ITO glass was rinsed with distilled water and dried. The gold electrodeposit on the ITO glass was investigated with SEM (Hitachi TM3030),

XRD (Rigaku Ultima), and EDX (Shimadzu 8000). The conventional XRD with $\text{CuK}\alpha$ radiation was applied to the gold electrodeposit using a standard θ - 2θ diffractometer with a monochromator of carbon.

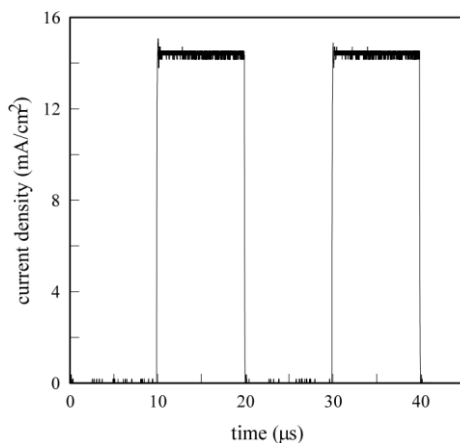


Figure 1. Rectangular pulse current having an amplitude of 14.4 mA/cm^2 and a frequency of 50 kHz.

3. EXPERIMENTAL RESULTS AND DISCUSSION

3.1 Star-like gold electrodeposit

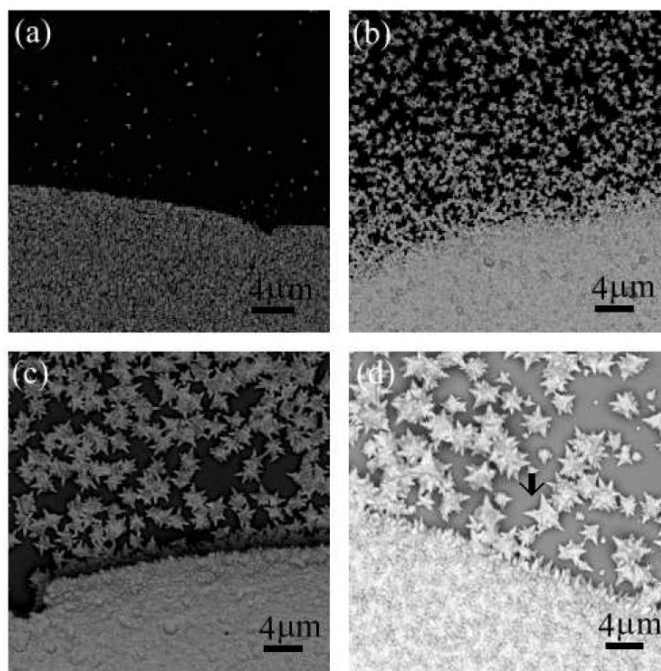


Figure 2. SEM images of a gold thin film and star-like gold electrodeposits generated near its edge at a deposition time of (a) 15 s, (b) 90 s, (c) 180 s, and (d) 270 s. The gold electrodeposits were generated at a solution temperature of 303 K and at a rectangular pulse current amplitude of 7.7 mA/cm^2 .

Figure 2 shows SEM images of developing gold islands and gold thin film at a solution temperature of 303 K. A small number of the gold islands that exit far from the gold thin film at a deposition time of 15 s are shown in Fig. 2 (a). The dimension and the number of the gold islands increase with a deposition time. The gold island is a concave polygon with several horns and a star-like appearance with geometrical symmetry. In this study, we call the gold island a star-like gold electrodeposit. As shown in Fig. 2 (b), (c), and (d), the star-like gold electrodeposits that are located in the immediate vicinity of the gold thin film are incorporated into the gold thin film and form an edge of the gold thin film. Many horns on the edge indicate that they were a portion of the star-like gold electrodeposit prior to incorporation into the gold thin film.

In Fig. 2 (d), the arrow shows a star-like gold electrodeposit with a pentagonal symmetry. The central angle about 72 degrees is consistent with that of the pentagon. However, many star-like gold electrodeposits exhibit a more complicated configuration having more than five horns. The horn is thought to be bounded by crystallographic planes with higher Mirror indices [4]. This indicates that a principle of the total surface energy minimum dominates the surface configuration.

Table 1. The atomic element in the gold thin film investigated with EDX. The gold thin film was electrodeposited at a solution temperature of 303 K and an amplitude of 14.4 mA/cm².

element(wt%) deposition time(s)	Au	Si	K	Ca	In	Residual quantities
15	9.7	40.1	15.5	30.8	0.9	3.0
45	48.8	11.3	10.6	24.7	2.7	1.9
90	81.8	0	3.4	9.7	2.9	2.2
180	96.0	0	0.2	1.2	1.9	0.7
270	97.5	0	0.2	0.6	1.3	0.4

The chemical components in the star-like gold electrodeposit and the gold thin film were investigated with EDX. Table 1 shows a list of the elements detected in the gold electrodeposit on the ITO glass. The detected elements, Si, K, Ca, and In result from the characteristic X-ray excited from the soda glass plate and the ITO. No sulfur included in the gold electrodeposition solution (AuNa₃O₃S₂) is observed. This is the advantage using a pulse current electrodeposition [16]. The content of gold increases with the deposition time. These results show that the electrodeposit is purely made of gold.

SEM images of gold thin films comprising of the star-like gold electrodeposits are shown in Fig. 3 as well as those in Fig. 2. A great number of pores that appear as black dots in Fig. 3 (a) are observed in the surface of the gold thin film at a deposition time of 45 s. The mesostructured pores in gold materials are known to indicate an extraordinary property in catalysis [1]. As shown in Fig. 3 (b), the number of pores decreases with the deposition time.

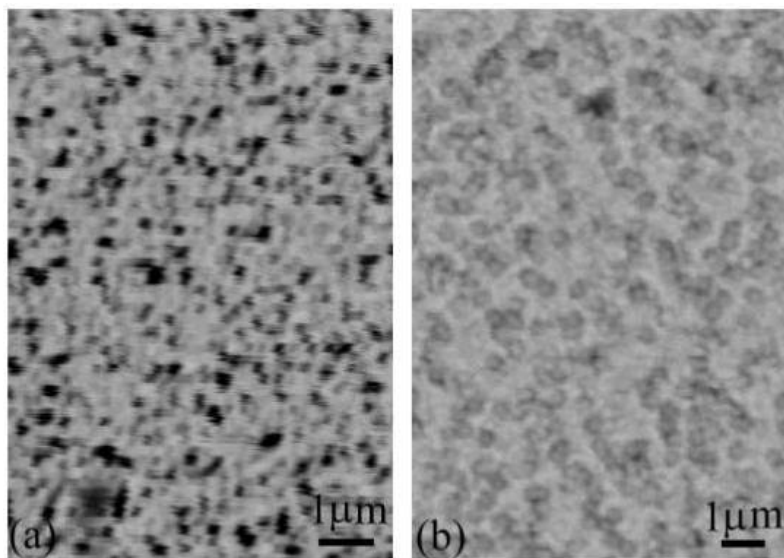


Figure 3. SEM images of gold thin films electrodeposited at a solution temperature of 303 K, a rectangular pulse current amplitude of 7.7 mA/cm^2 , and a deposition time of (a) 45 s and (b) 180 s.

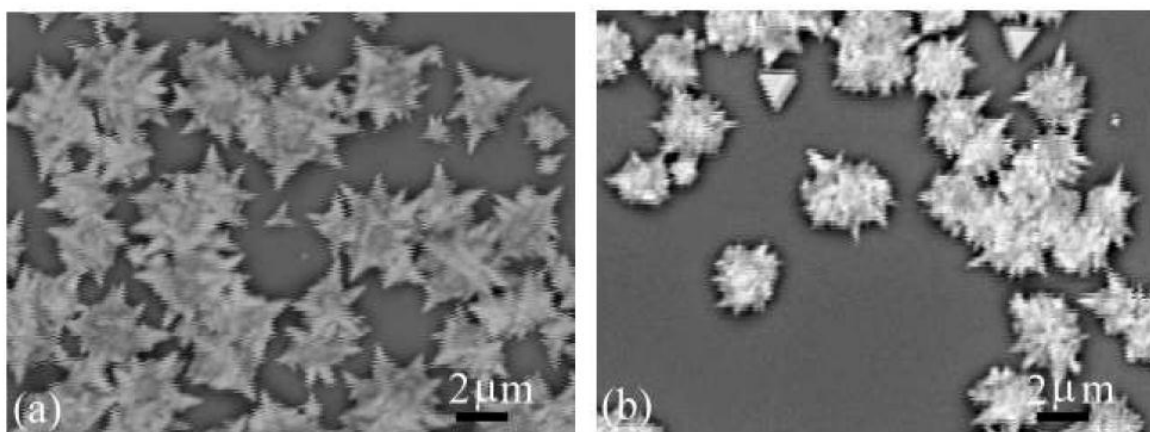


Figure 4. SEM images of star-like gold electrodeposits generated at a rectangular pulse current amplitude of 7.7 mA/cm^2 and at a solution temperature of (a) 303 K and (b) 323 K.

When the solution temperature is raised up from 303 K to 323 K, the configuration of the star-like gold electrodeposit changes as shown in Fig. 4 (b). In comparison with Fig. 4 (a), the horn grown at 323 K is shorter than that at 303 K. As the diffusion of gold atom accelerates with an increase in temperature, the horn changes into a blunt and short tip. In addition, triangle-shaped gold electrodeposits appear among the star-like gold electrodeposit electrodeposit in Fig. 4 (b). The surface energy of metals decreases with temperature [17]. According to the Monte Carlo simulation [18], the anisotropy of the Cu surface energy increases with temperature. In this study, with an increase in temperature the surface configuration of gold also seems to approach a simpler configuration, however, the surface energy minimum still determines the surface morphology.

3.2 Pyramid-like gold electrodeposit

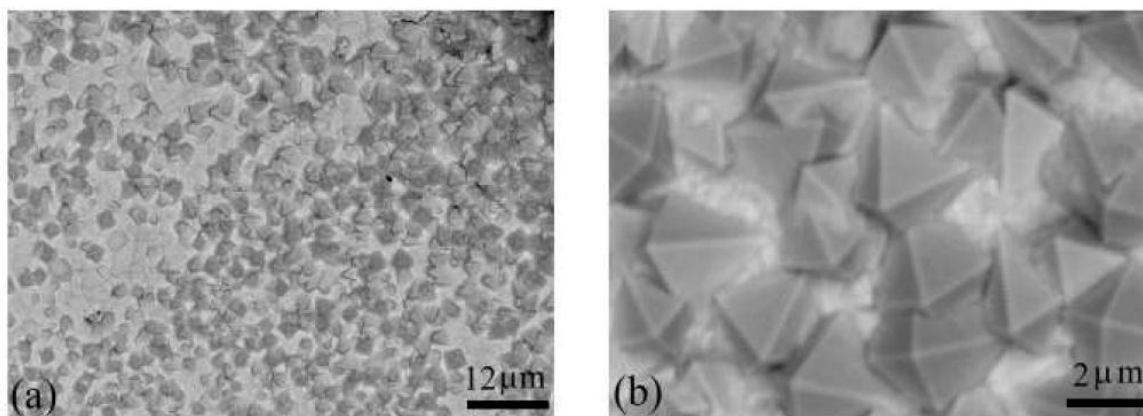


Figure 5. SEM images of pyramid-like gold electrodeposits comprising four triangular (111) planes. These electrodeposits were generated at a solution temperature of 323 K and a rectangular pulse current amplitude of 14.4 mA/cm². (a) Surface image comprising the pyramid-like gold electrodeposit. (b) Pyramid-like gold electrodeposit.

Eight (111) planes form a bipyramid. A truncated bipyramid comprising four triangular (111) planes and one square base is called a regular pyramid. The intersection edge of the two (111) planes is represented as {110} in the Miller index. In Fig. 5, the interior angle between the intersection edges of the triangle has about 60 degrees. Hence, the electrodeposit can be called a pyramid-like gold electrodeposit. The pyramid-like gold electrodeposit appears when the amplitude of the rectangular pulse current increases from 7.7 to 14.4 mA/cm².

The crystallographic Miller index of a base plane is investigated with XRD. Figure 6 shows a typical XRD chart of the gold electrodeposit. Bragg's law angles of diffraction peaks for the (111), (200), (220), and (222) and (311) plane are consistent with each standard diffraction peak of gold [19]. As no other peak except for gold is observed, the electrodeposit is purely made of gold as well as the result by EDX. In order to make clear dominant crystallographic planes in the gold electrodeposit, which are parallel to the ITO glass, the texture coefficient [19] $T(hkl)$ defined by

$$T(hkl) = \frac{I(hkl)_i / I_o(hkl)_i}{\sum_N I(hkl)_i / I_o(hkl)_i}, \quad (1)$$

where $I(hkl)_i$ is the measured intensity of the (hkl) diffraction, $I_o(hkl)_i$ is the standard intensity of polycrystalline gold [20], and N is the total number of a diffraction peak, is used.

Figure 7 shows the time-dependence of the texture coefficient for the (111), (200), (220), and (311) plane each. At an initial stage, the (111) plane that has the lowest surface energy in FCC metals is dominant. However, as electrodeposition proceeds, the (110) plane becomes dominant instead of the (111) plane, that is, the texture change takes place. The (110) plane has the largest surface energy among the (111), (100) and (110) plane. On the other hand, the (110) has the largest exchange current density among the (111), (100) and (110) plane [13]. For the larger rectangular current pulse amplitude, in other words, at the far-from equilibrium growth, the plane with the largest growth rate

dominates the crystal habit. Hence, the (110) with the largest exchange current density becomes dominant. However, the gold electrodeposit in Fig. 5 is covered with the pyramid-like electrodeposit comprising the four (111) planes that have the smallest surface energy. This indicates that in this study the surface morphology still obeys the surface energy minimum.

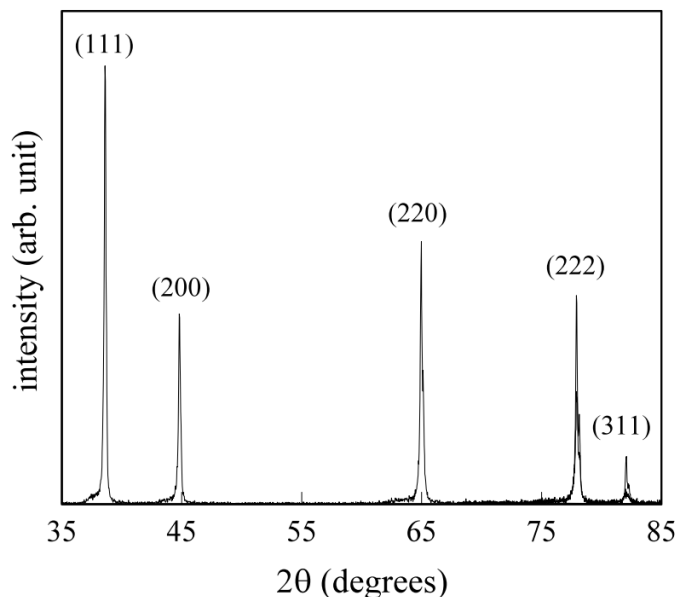


Figure 6. A typical XRD chart of the gold thin film. The gold electrodeposit was generated at a deposition time of 180 s, a solution temperature of 323 K, and a rectangular pulse current amplitude of 14.4 mA/cm².

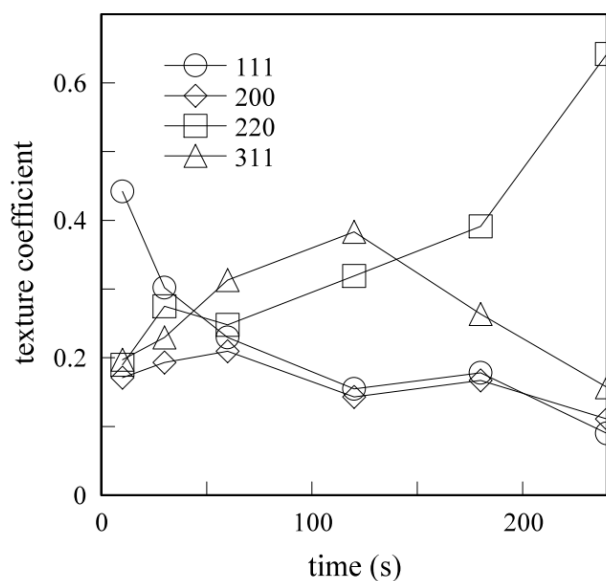


Figure 7. Texture coefficient for four crystallographic planes. The gold thin film electrodeposited at a solution temperature of 323 K and an amplitude of 14.4 mA/cm².

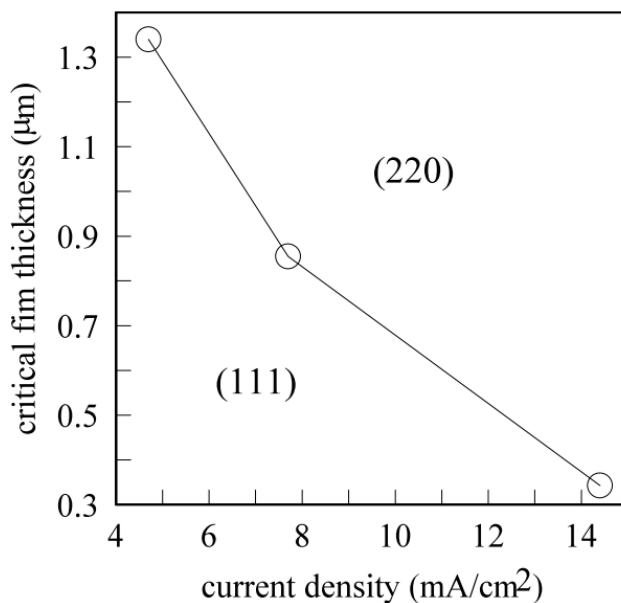


Figure 8. Texture change dependent on the rectangular pulse current amplitude. The (111) and (110) denote each dominant plane parallel to the ITO glass.

In addition, in some pyramid-like electrodeposits in Fig. 5 (a), a line joining the apex and centroid of the base is perpendicular to the base. However, the line in most pyramid-like electrodeposits is not perpendicular to the base but tilted. This indicates that the base is not the (100) plane.

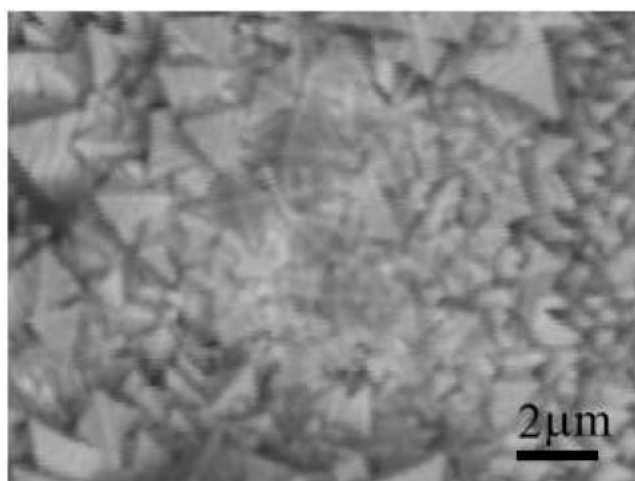


Figure 9. SEM image of pyramid-like gold electrodeposit generated at a solution temperature of 303 K and a rectangular pulse current amplitude of 14.4 mA/cm².

Using Fig. 7, a film thickness at the deposition time at which the line of the (111) texture coefficient and that of the (220) texture coefficient intersect can be defined as a critical film thickness. Figure 8 shows the texture change dependent on the rectangular current pulse amplitude. The dominant region can be divided by the critical film thickness. As the pulse current amplitude increases, the texture change from the (111) to the (110) takes place at a smaller critical film thickness. At higher

rectangular pulse amplitude, the crystallographic plane with a higher growth rate is needed to grow. Hence, the (110) plane with the largest exchange current density is thought to appear [21].

When the solution temperature decreases from 323 to 303 K and a rectangular pulse current of 14.4 mA/cm² is held, the morphology of the gold electrodeposit changes as shown in Fig. 9. The number of the pyramid-like gold electrodeposit remarkably increases.

4. CONCLUSIONS

Two kinds of the anisotropic mesostructured gold electrodeposit, i.e., the star-like and pyramid-like gold electrodeposits were generated using a rectangular pulse current technique. As the rectangular current pulse amplitude and the solution temperature increase, the star-like gold electrodeposit changes into the pyramid-like gold electrodeposit. The gold electrodeposit is purely made of gold. The gold thin film comprising of the star-like gold electrodeposit is found to have mesostructured pores. The texture change from the (111) plane to the (110) plane takes place, whereas the surface configuration obeys the surface energy minimum.

ACKNOWLEDGEMENTS

The author deeply appreciates Mr. S. Shiroma for his help in the experimental setup.

References

1. P. R. Sajanlal and T. Pradeep, *Nano Res.*, 2 (2009) 306.
2. S-J. Park, M-L. Seol, S-B. Jeon, D. Kim, D. Lee, and Y-K. Choi, *Sci. Rep.*, 5 (2015) 13866.
3. X. Liu, N. Wu, B. H. Wunsch, R. J. Barsotti Jr., and F. Stellacci, *Small*, 2 (2006) 1046.
4. H. Katz-Boon, C. J. Rossouw, M. Weyland, A. M. Funston, P. Mulvaney, and J. Etheridge, *Nano Lett.*, 11 (2011) 273.
5. C. Langlois, P. Benzo, R. Arenal, M. Benoit, J. Nicolai, N. Combe, A. Ponchet, and M. J. Casanova, *Nano Lett.*, 15 (2015) 5075.
6. Y. Q. Wang, W. S. Liang, C. Y. Geng, *J. Nanopart. Res.*, 12 (2009) 655.
7. S. Dimitrijević, M. R. -Vujasinović, and V. Trujić, *Int. J. Electrochem. Sci.*, 8 (2013) 6620.
8. L. Wei, D. Kai, Z. Lin, X. Jiang, Z. Chao, Z. Yunwang, Z. Lan, Y. Qiang, *Electrochimica Acta* 95 (2013) 179.
9. A. I. de Sâ, S. Eugénio, S. Quaresma, C.M. Rangel, R. Vilar, *Thin Solid Films* 519 (2011) 6278.
10. E. Ringe, R. P. V. Duyne, and L. D. Marks, *Nano Lett.*, 11 (2011) 3399.
11. N. E. Singh-Miller and N. Marzari, *Phys. Rev. B*, 80 (2009) 235407.
12. C. Herring, *Phys. Rev.*, 82 (1951) 87.
13. G. J. Brug, M. S-Rehbach, and J. H. Sluyters, *J. Electroanal. Chem.*, 181 (1984) 245.
14. N. M. Marković, B. N. Grgur, and P. N. Ross, *J. Phys. Chem. B*, 101 (1997) 5405.
15. M. J. Liew, S. Roy, and K. Scott, *Green. Chem.*, 5 (2003) 376.
16. Ch. J. Raub and A. Knödler, *Gold Bull.*, 10 (1977) 38.
17. S. Kristyian and J. Giber, *Surf. Sci.*, 201 (1988) L532.
18. T. Frolov and Y. Mishin, *Phys. Rev. B*, 79 (2009) 045430.
19. M. Saitou, *Int. J. Electrochem. Sci.*, 11 (2016) 1651.
20. JCPDS-ICDD Card No. 04-0784.

21. M. Mallik, A. Mitra, S. Sengupta, K. Das, R. N. Ghosh, and S. Das, *Cryst. Growth Des.*, 14 (2014) 6542.

© 2016 The Authors. Published by ESG (www.electrochemsci.org). This article is an open access article distributed under the terms and conditions of the Creative Commons Attribution license (<http://creativecommons.org/licenses/by/4.0/>).